
Resolving Representation Ambiguity in Feedforward Novel View Synthesis Transformer via Semantic-Spatial Decoupling

Yihang Wu^{1,2*} Yihang Sun^{3*} Shaofeng Zhang⁴

Zuxuan Wu^{1,2} Junchi Yan^{3✉} Xiaosong Jia^{1,2✉} Yu-gang Jiang^{1,2}

¹Institute of Trustworthy Embodied Artificial Intelligence (TEAI), Fudan University

²Shanghai Key Laboratory of Multimodal Embodied AI

³Sch. of Artificial Intelligence & Sch. of Computer Science, Shanghai Jiao Tong University

⁴University of Science and Technology of China

* Equal Contributions ✉ Correspondence Author

Abstract

Transformer-based models have advanced feedforward novel view synthesis (NVS). Current architectures such as GS-LRM and LVSM mix semantic information (e.g., RGB) and spatial information (e.g., Plücker rays) into a shared feature space. Since Plücker rays naturally carry lattice-like spatial structure, these designs can make the spatial bias interfere with appearance representation and degrade rendering fidelity. To this end, we propose to **decouple the representation of feedforward NVS transformers into separate semantic and spatial tokens**. The decoupled design keeps semantic and spatial information explicit in their branches while preserving cross-branch interaction through shared attention routing. Built on this design, we introduce optional categorized supervision and bidirectional modulation: the former provides branch-specific training signals, while the latter improves interaction between the two branches. Notably, the base decoupled design introduces virtually zero additional inference latency due to its architectural design. The proposed designs achieve consistent improvements, demonstrating effectiveness across decoder-only and encoder-decoder feedforward NVS models.

Project page: https://hangzay.github.io/ssd_lvsm/

1 Introduction

Novel View Synthesis (NVS) has undergone a fundamental paradigm shift, moving from per-scene optimization [23, 16] to generalizable feedforward inference powered by Large Reconstruction Models (LRMs) [10]. Transformer-based architectures like GS-LRM [41] and LVSM [13] typically adopt a unified token approach, where semantic features (RGB patches) and spatial features (Plücker rays) are concatenated and projected into a shared latent space. However, since Plücker rays naturally carry lattice-like spatial structure, such forced coupling can make spatial bias interfere with appearance representation. Additionally, we find that this entanglement yields grid-like distortion [27] on features and leads to degraded rendering, as in Fig. 4.

Inspired by register tokens [6] in ViTs, we first introduce registers to provide extra storage slots, but this control does not resolve the issue. In this work, we propose to **decouple semantic and spatial**

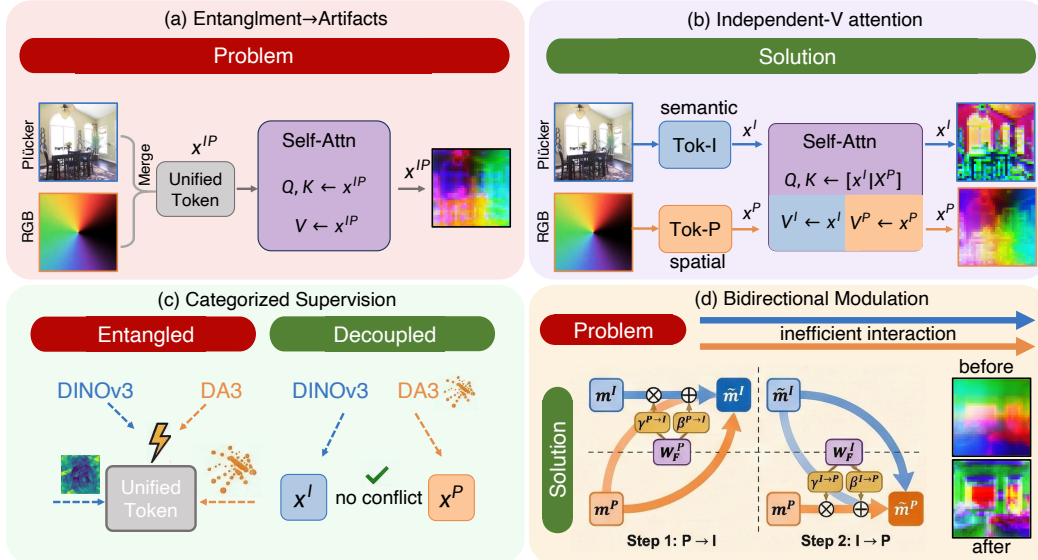


Figure 1: **Overview.** In this work, we identify that mixing RGB and Plücker-ray information in a shared feature space can make spatial bias interfere with appearance representation. We decouple the two information streams while preserving cross-branch interaction to enhance rendering.

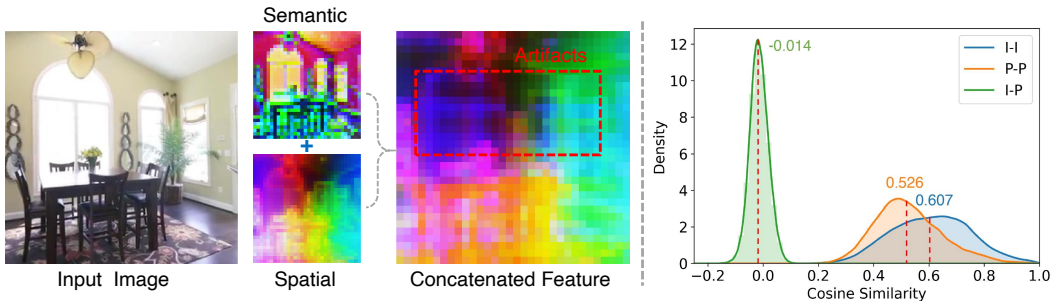


Figure 2: **Feature Coupling and Cosine Similarity.** Left: Semantic and spatial features are structured separately, while their concatenation exposes grid-like Plücker-related artifacts. Right: We sample vector pairs to estimate cosine similarity distributions for I-I (semantic), P-P (spatial), and I-P (cross-branch). Dashed lines indicate the mean of each group.

tokens, redesigning the Transformer representation space to preserve semantic and spatial feature independence while facilitating cross-stream context exchange. The core architectural change is full-pipeline decoupling Transformer by **Independent-V Attention mechanism** that shares query-key routing for coordination while maintaining two separate value streams. Based on this decoupled representation, we further introduce optional categorized supervision and bidirectional modulation as auxiliary designs. The supervision terms provide branch-specific training signals and are removed at inference, while modulation improves controlled cross-branch conditioning.

Notably, the proposed decoupled design incurs virtually zero additional inference latency while bringing a gain over the entangled baseline. Optional supervision and modulation further improve performance, reaching a 1.1 dB PSNR gain with an 8% inference-time increase. Extensive experiments across architectures and datasets validate the effectiveness of the proposed approach.

2 Related Work

Feedforward Novel View Synthesis. NVS has progressed from image-based rendering [7] and per-scene neural optimization [23, 16] to feed-forward approaches. Early methods [39, 32, 5] conditioned NeRF networks on pixel-aligned features but retained explicit 3D inductive biases, which transformer-based LRMs [10, 41, 46] replaced with data-driven priors. Geometry-free sequence-to-sequence models [13, 12, 44, 11, 20] further simplify NVS into direct token-level prediction. Despite these advances, recent feedforward NVS transformers commonly encode semantic appearance and

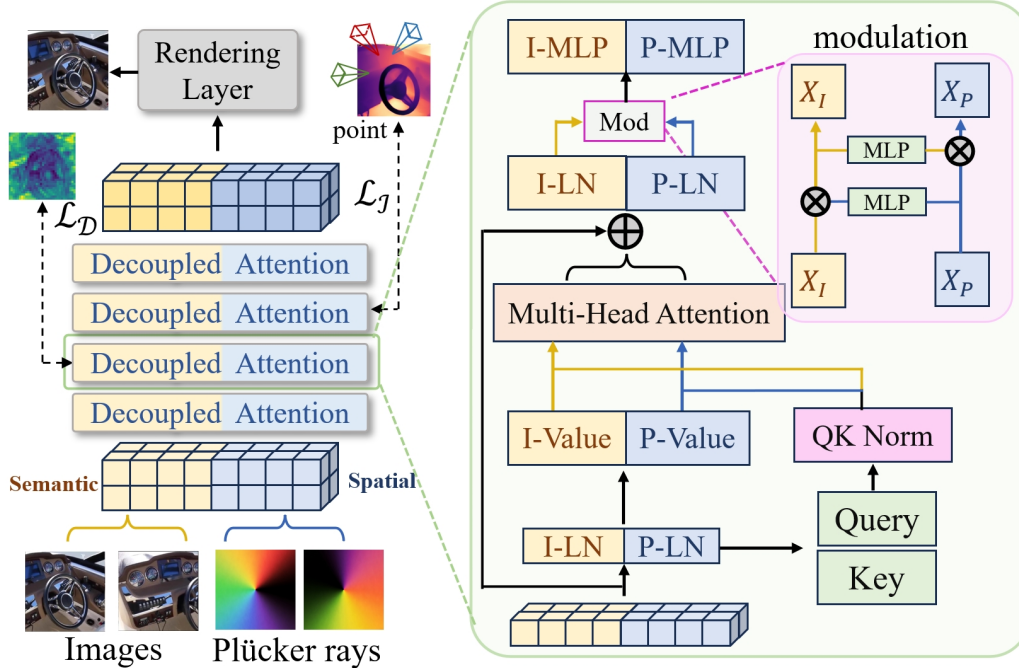


Figure 3: **Semantic-Spatial Decoupled Architecture for Feedforward NVS.** Semantic tokens (I) from RGB and spatial tokens (P) from Plücker rays pass through decoupled-attention blocks. Attention shares query-key interactions while using independent value projections to preserve heterogeneous representations. Bidirectional modulation further enables cross-stream conditioning, spatial geometry within unified tokens. Our work addresses the resulting intra-token representation ambiguity, complementary to concurrent efforts on improved camera conditioning [36].

Token Dynamics and Feature Artifacts in Vision Transformers. ViTs [9] exhibit representational artifacts such as grid-like patterns linked to positional encoding [27] and high-norm outlier tokens associated with implicit memory storage [6]. Register tokens provide dedicated storage slots for such outlier behavior [6, 17, 22], which is also related to attention sink phenomena in language models [1]. In NVS transformers, however, each patch token is also bound to a camera ray, so feature artifacts are coupled with semantic-spatial mixing rather than token dynamics alone. This motivates us to separate semantic and spatial representations instead of relying only on additional register tokens.

Representation Alignment. The DINO series [4, 24, 28] has shown that self-supervised ViT features provide useful visual representations for downstream generative models. REPA [40] and its variants [30, 18, 43] align hidden states with such features to improve generative training, while iREPA [29] emphasizes fine-grained spatial correspondence. Applying this supervision to unified NVS tokens can mix semantic and geometric objectives. We therefore use iREPA with DINOv3 as branch-specific supervision for the decoupled semantic stream.

Geometric Priors for 3D Understanding. Monocular and multi-view depth estimation has matured into a family of large-scale foundation models [2, 37, 38, 3, 33, 34]. DA3 [19] extends this line to multi-view consistent 3D point-map prediction. We use its outputs as training-time geometric supervision for the decoupled spatial stream, grounding spatial representations without adding inference-time geometry modules.

3 Method

3.1 Preliminary

Given N posed input images $\{(\mathbf{I}_i, \mathbf{E}_i, \mathbf{K}_i)\}_{i=1}^N$ and M target poses $\{(\mathbf{E}_j, \mathbf{K}_j)\}_{j=1}^M$, feedforward NVS renders $\{\hat{\mathbf{I}}_j\}_{j=1}^M$ in a single forward pass, where $\mathbf{I}_i \in \mathbb{R}^{H \times W \times 3}$ is the input RGB image, $\mathbf{E}_i, \mathbf{K}_i \in \mathbb{R}^{4 \times 4}$ are the extrinsic and intrinsic matrices, and $\hat{\mathbf{I}}_j \in \mathbb{R}^{H \times W \times 3}$ is the rendered output. In this work, we adopt LVSM [13] as the baseline. The camera viewpoints are encoded as Plücker ray

maps [26] $\pi_i \in \mathbb{R}^{6 \times H \times W}$. Each input view is divided into $N_p = HW/p^2$ non-overlapping patches of size $p \times p$; the RGB and Plücker patch sequences, denoted \mathbf{I}_i^P and π_i^P , are *concatenated along the channel dimension* and projected into the D -dimensional token space, while target tokens are Plücker patches alone:

$$\mathbf{t}_i = \text{MLP}_{\text{in}}(\text{concat}(\mathbf{I}_i^P, \pi_i^P)) \in \mathbb{R}^{N_p \times D}, \quad \mathbf{q}_j = \text{MLP}_{\text{tgt}}(\pi_j^P) \in \mathbb{R}^{N_p \times D}. \quad (1)$$

All tokens are then concatenated and processed by L layers of full self-attention, after which target features are fed into the rendering head.

3.2 Decoupled Semantic and Spatial Tokens

Decoupled Tokenization. As shown in Fig. 3, we replace the modality-mixing input projection in LVSM with two separate tokenizers for semantic appearance and spatial geometry. For each input view, RGB patches \mathbf{I}_i^P and Plücker-ray patches π_i^P are tokenized into a semantic branch (I -branch) and a spatial branch (P -branch):

$$\mathbf{x}_i^I = \text{Tok}_I(\mathbf{I}_i^P) \in \mathbb{R}^{N_p \times \frac{D}{2}}, \quad \mathbf{x}_i^P = \text{Tok}_P(\pi_i^P) \in \mathbb{R}^{N_p \times \frac{D}{2}}. \quad (2)$$

For each target view, no RGB observation is available, so we initialize the target semantic branch with zeros and tokenize the target Plücker-ray patches into the spatial branch:

$$\mathbf{y}_j^I = \mathbf{0} \in \mathbb{R}^{N_p \times \frac{D}{2}}, \quad \mathbf{y}_j^P = \text{Tok}_P^{\text{tgt}}(\pi_j^P) \in \mathbb{R}^{N_p \times \frac{D}{2}}. \quad (3)$$

The full input and target tokens are then formed by concatenating their I -branch and P -branch features. The total token dimension therefore remains the same as the original LVSM token, while the branch partition is preserved throughout the Transformer blocks.

Independent-V Attention. Each decoupled Transformer block keeps query-key (Q/K) routing on the full token, but uses branch-specific value and output projections. With branch-wise pre-normalized inputs $\bar{\mathbf{x}}^I$ and $\bar{\mathbf{x}}^P$, let $\bar{\mathbf{x}} = \text{concat}(\bar{\mathbf{x}}^I, \bar{\mathbf{x}}^P)$. We compute

$$\mathbf{q} = \bar{\mathbf{x}}\mathbf{W}_q, \quad \mathbf{k} = \bar{\mathbf{x}}\mathbf{W}_k, \quad \mathbf{v}^I = \bar{\mathbf{x}}^I\mathbf{W}_v^I, \quad \mathbf{v}^P = \bar{\mathbf{x}}^P\mathbf{W}_v^P. \quad (4)$$

Here \mathbf{W}_q and \mathbf{W}_k project the full token to Q/K, while \mathbf{W}_v^I and \mathbf{W}_v^P project the two value streams separately. The shared attention map is

$$\mathbf{A} = \text{softmax}\left(\frac{\mathbf{q}\mathbf{k}^\top}{\sqrt{d_h}}\right), \quad (5)$$

where d_h is the per-head Q/K dimension. The same attention map is applied to the two branch-specific value streams and followed by branch-specific output projections:

$$\mathbf{o} = \text{concat}(\mathbf{W}_o^I(\mathbf{A}\mathbf{v}^I), \mathbf{W}_o^P(\mathbf{A}\mathbf{v}^P)). \quad (6)$$

where \mathbf{W}_o^I and \mathbf{W}_o^P are the output projections for the two branches. After attention, the I -branch and P -branch are processed by branch-specific layer normalization (LN) and half-dimensional feed-forward networks (FFNs), then concatenated back to a D -dimensional token. Thus, the block preserves full-token interaction through shared Q/K while keeping value updates and FFN transformations branch-specific. The qualitative feature progression in Fig. 4 visualizes the resulting change in intermediate representations, with detailed analysis provided in Sec. 4.4.

3.3 Optional Categorized Supervision

The decoupled representation enables optional categorized supervision for the I -branch and P -branch.

Semantic Alignment via iREPA with DINOv3. For the I -branch, we align intermediate semantic features with frozen DINOv3 features using an iREPA-style representation alignment [29]. Let $\mathbf{x}_{k_I}^I$ denote the I -branch feature at layer k_I , $f_{\text{DINO}}(\mathbf{I})$ denote the DINOv3 teacher feature, $\text{SN}(\cdot)$ denote spatial normalization, and h_ϕ denote the semantic projection head. The semantic supervision is

$$\mathcal{L}_{\text{iREPA}} = \text{SmoothL1}(h_\phi(\text{SN}(\mathbf{x}_{k_I}^I)), f_{\text{DINO}}(\mathbf{I})). \quad (7)$$

For a token feature \mathbf{z} , spatial normalization is defined as

$$\text{SN}(\mathbf{z}) = \frac{\mathbf{z} - \gamma\mu(\mathbf{z})}{\sigma(\mathbf{z}) + \epsilon}, \quad (8)$$

where $\mu(\mathbf{z})$ and $\sigma(\mathbf{z})$ are computed over the token dimension, γ is a normalization coefficient, and ϵ is a small constant for numerical stability. Inspired by iREPA, this normalization emphasizes local feature variation before alignment. Both h_ϕ and the DINOv3 teacher are discarded at inference.

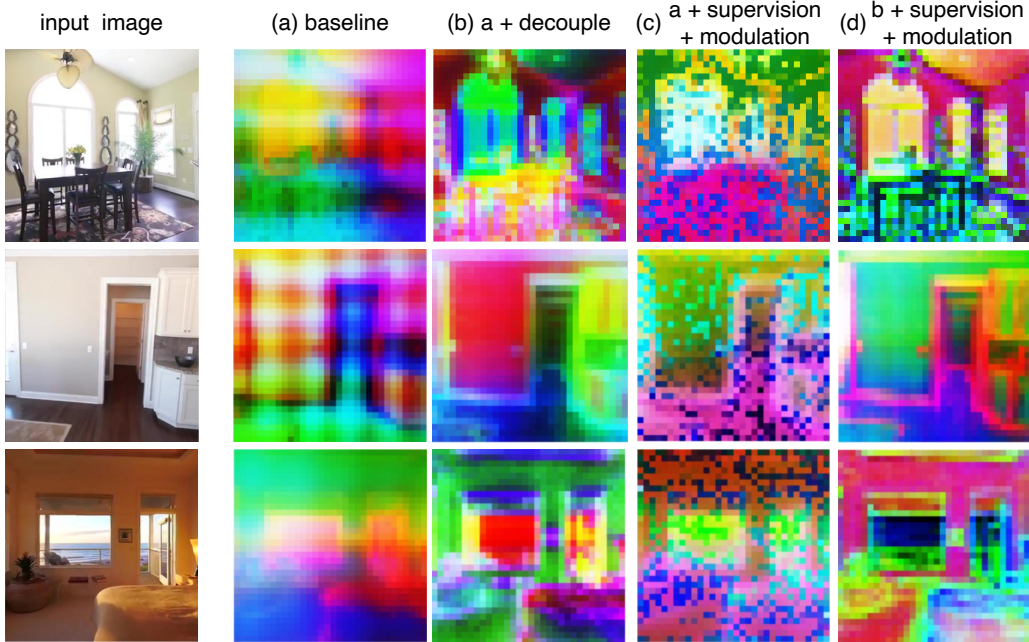


Figure 4: **Feature Map Comparison across Model Variants.** We visualize intermediate feature maps from middle Transformer layers: decoupling produces more structured representations, while supervision and modulation are most effective when applied on top of the decoupled token design. **Geometric Consistency of the Spatial Branch.** For the P -branch, we use DA3-derived geometry [19] to construct visible cross-view correspondences. Specifically, source-view 3D points are projected into target views with the aligned camera parameters; when multiple source points map to the same target location, z-buffering keeps the point with the smallest target-view depth and filters occluded matches. Let Ω_j be the resulting correspondence set for target view j , where $(i, u, v) \in \Omega_j$ matches source location u in view i to target location v in view j . We supervise the spatial branch with feature cosine consistency:

$$\mathcal{L}_{\text{geo}} = \frac{1}{|\mathcal{J}|} \sum_{j \in \mathcal{J}} \frac{1}{|\Omega_j|} \sum_{(i, u, v) \in \Omega_j} (1 - \cos(\mathbf{x}_{k_P, i, u}^P, \mathbf{x}_{k_P, j, v}^P)), \quad (9)$$

where \mathcal{J} denotes target views with valid correspondences, $\mathbf{x}_{k_P, i, u}^P$ and $\mathbf{x}_{k_P, j, v}^P$ denote P -branch features at layer k_P for the matched locations, and $\cos(\cdot, \cdot)$ denotes cosine similarity. The cached DA3 geometry is used to build correspondence supervision during training and is not used at inference.

3.4 Optional Bidirectional Feature Modulation

Bidirectional modulation is an optional refinement on top of the decoupled Transformer block. It uses cross-branch conditioning [25] after layer normalization and before the branch-specific FFNs.

Spatial \rightarrow Semantic. Let \mathbf{m}^I and \mathbf{m}^P denote the layer-normalized attention outputs of the I and P branches respectively, i.e., the inputs to their corresponding FFNs. The spatial representation \mathbf{m}^P generates scale and shift parameters that modulate the semantic branch:

$$(\gamma^{P \rightarrow I}, \beta^{P \rightarrow I}) = \mathbf{W}_F^P \mathbf{m}^P, \quad \tilde{\mathbf{m}}^I = \gamma^{P \rightarrow I} \odot \mathbf{m}^I + \beta^{P \rightarrow I}. \quad (10)$$

This step lets spatial cues such as view direction and ray geometry condition the semantic update without merging spatial channels into the semantic representation.

Semantic \rightarrow Spatial. The modulated semantic representation $\tilde{\mathbf{m}}^I$ then generates the reverse affine parameters for the spatial branch:

$$(\gamma^{I \rightarrow P}, \beta^{I \rightarrow P}) = \mathbf{W}_F^I \tilde{\mathbf{m}}^I, \quad \tilde{\mathbf{m}}^P = \gamma^{I \rightarrow P} \odot \mathbf{m}^P + \beta^{I \rightarrow P}. \quad (11)$$

The branch-specific FFNs are then applied to $\tilde{\mathbf{m}}^I$ and $\tilde{\mathbf{m}}^P$ separately. Thus, modulation provides controlled bidirectional conditioning while preserving the decoupled representation.

Here \mathbf{W}_F^P and \mathbf{W}_F^I are learnable linear generators, and γ, β are the predicted scale and shift parameters. We initialize the generators as an identity modulation, with zero weights, scale bias

Table 1: **Main Results and Core Component Control.** Left: controlled baselines across architectures and datasets. Obj: objaverse; Right: LVSM Decoder-Only component control on RealEstate10K. Sup: categorized supervision; Mod: bidirectional modulation.

Arch.	Dataset	Model	PSNR \uparrow	SSIM \uparrow	LPIPS \downarrow	Configuration	PSNR \uparrow	SSIM \uparrow	LPIPS \downarrow
Dec-Only	RE10K	Baseline	26.10	0.839	0.144	Decouple	26.70	0.851	0.138
		Ours(full)	27.21	0.869	0.125				
Dec-Only	Obj	Baseline	23.75	0.864	0.150	Decouple + Sup	26.91	0.857	0.134
		Ours(full)	26.46	0.899	0.101	Decouple + Mod	27.06	0.860	0.131
Enc-Dec	RE10K	Baseline	24.06	0.775	0.206	Decouple + Sup + Mod	27.21	0.869	0.125
		Ours(full)	25.31	0.806	0.154				

initialized to one, and shift bias initialized to zero. Therefore, enabling modulation starts from the original decoupled block and learns cross-branch corrections only when they are useful.

3.5 Training Objective

The base decoupled model is trained with the RGB reconstruction loss. When optional categorized supervision is enabled, the objective becomes

$$\mathcal{L} = \mathcal{L}_{\text{RGB}} + \lambda_I \mathcal{L}_{\text{iREPA}} + \lambda_P \mathcal{L}_{\text{geo}}. \quad (12)$$

Here $\mathcal{L}_{\text{iREPA}}$ and \mathcal{L}_{geo} constrain the I -branch and P -branch only during training. Implementation details and loss weights are provided in Appendix A.

4 Experiments

4.1 Datasets

Scene-Level. For scene-level, we use RealEstate10K [45], which aggregates over 80K video clips of diverse indoor and outdoor environments collected from YouTube. The dataset provides large-scale real-world scenes with varied viewpoints and camera motions. Train and test splits follow LVSM [13].

Object-Level. Object-level experiments use Objaverse [8] for training, with 730K objects each rendered at 32 viewpoints using the GS-LRM [41] pipeline. Evaluation is performed on the Objaverse test split. At test time, each object is presented with 4 structured input views, and performance is measured on 10 held-out target views sampled at random, following the protocol of LVSM [13].

4.2 Implementation Details

Model Configurations. We adopt two feedforward NVS architectures as backbones: LVSM Decoder-Only [13], consisting of 12 Transformer layers, and LVSM Encoder-Decoder, comprising a 12-layer encoder paired with a 12-layer decoder. Both variants share a hidden dimension of 768.

Controlled Reimplementation. All baseline and decoupled models use the same codebase, data splits, view sampling protocol, resolution, and training budget. This controlled setting isolates the effect of semantic-spatial decoupling rather than reproducing maximum-scale backbone results. Detailed training settings are provided in Appendix A. We report PSNR, SSIM [35], and LPIPS [42] for all quantitative comparisons.

4.3 Comparison with Baselines

We compare each baseline architecture against its decoupled counterpart under a controlled setting, with results reported in Table 1. Across architectures and datasets, decoupling consistently improves rendering quality over the corresponding baselines. The component control shows that decoupling itself provides the main gain, while optional supervision and modulation bring additional improvements. Visual comparisons in Fig. 5 show more coherent structures and sharper details.

The Encoder-Decoder result in Table 1 indicates that the same decoupled design transfers to a 24-layer encoder-decoder backbone; detailed architecture and training settings are provided in Appendix C.

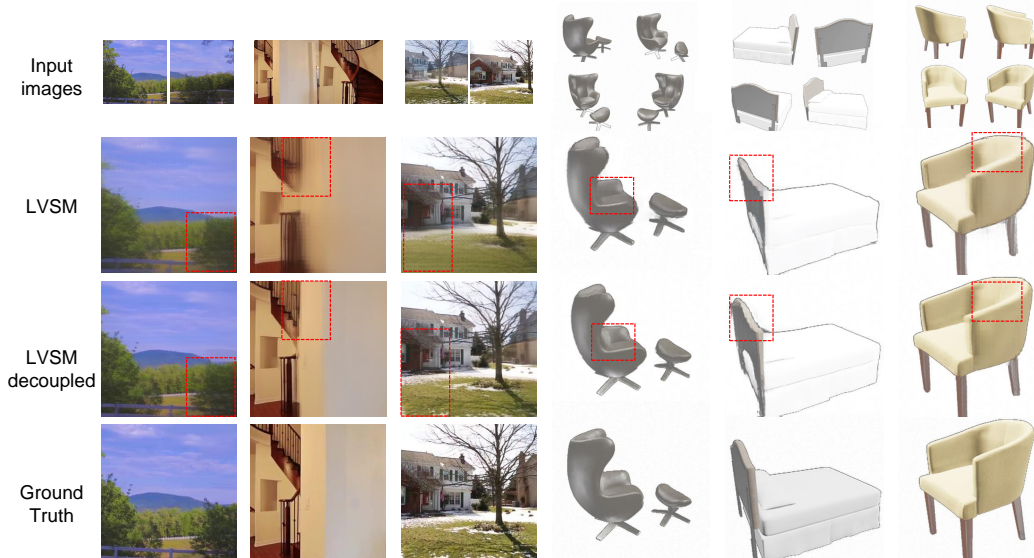


Figure 5: **Novel View Synthesis Visual Comparison.** Our decoupled model produces more coherent structures and sharper details.

Table 2: **Component Ablation.** Reg: register tokens. †Training diverged: result unavailable.

Configuration	PSNR↑	SSIM↑	LPIPS↓
Decoupling and Categorized Supervision			
Baseline	26.10	0.839	0.144
Baseline + Sup	26.02	0.831	0.148
Decouple	26.70	0.851	0.138
Decouple + Sup	26.91	0.857	0.134
Register Control			
Baseline + Reg	26.04	0.835	0.146
Baseline	26.10	0.839	0.144
Shared vs. Independent Q/K			
Independent-Q/K	25.90	0.832	0.148
Shared-Q/K	26.70	0.851	0.138
Modulation Placement			
Pre-Attn-LN†	—	—	—
Post-FFN	26.95	0.858	0.132
Post-Attn-LN/Pre-FFN	27.06	0.860	0.131
Effect of Bidirectional Modulation			
Baseline	26.10	0.839	0.144
Baseline + Mod	25.93	0.829	0.150
Decouple	26.70	0.851	0.138
Decouple + Mod	27.06	0.860	0.131
Cross-Branch Modulation Direction			
I→P only	26.80	0.853	0.136
P→I only	26.91	0.856	0.133
Decouple + Mod	27.06	0.860	0.131
LayerNorm Decoupling			
Joint-LN	26.01	0.830	0.149
Decouple	26.70	0.851	0.138
Full Configuration			
Decouple + Sup + Mod	27.21	0.869	0.125

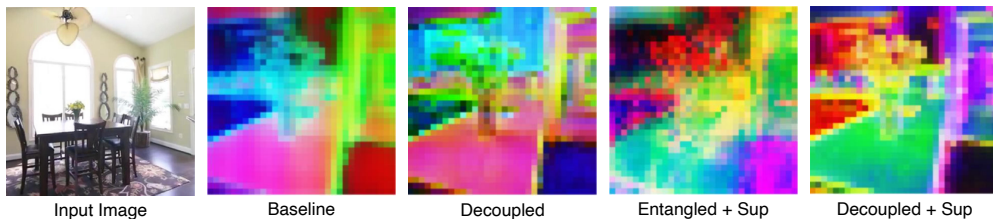


Figure 6: **Supervision Difference.** Categorized supervision benefits the decoupled model but harms the entangled baseline.

4.4 Ablation Study

Table 2 summarizes the component and control ablations. Unless otherwise specified, feature visualizations are taken from middle Transformer layers.

Decoupling and Categorized Supervision. In the entangled baseline, RGB and Plücker information share the same feature channels, so semantic alignment and geometric consistency are imposed on a mixed representation and do not improve rendering quality. After decoupling, the two objectives become well-defined: iREPA constrains the *I*-branch, while geometric correspondence constrains the

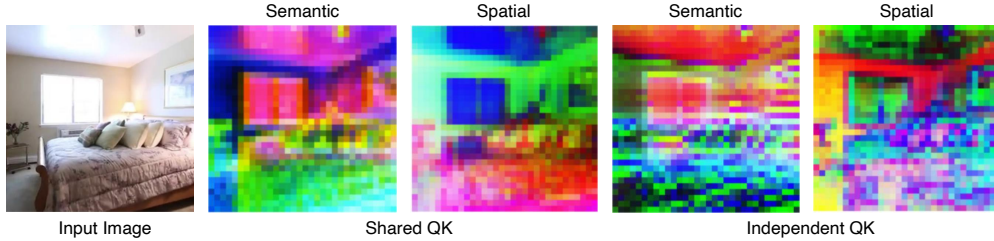


Figure 7: **Shared vs. Independent O/K.** Shared O/K with independent V yields better performance.

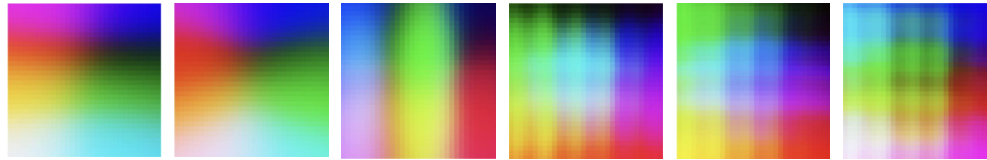


Figure 8: **Plücker-Only Inference Control.** Artifacts originate from the spatial ray representation. P -branch. Fig. 6 shows clearer semantic and geometric structures, confirming that supervision is secondary to, and enabled by, the decoupled representation.

Register Control. We add register tokens to the entangled baseline under the same setting to test whether the grid-like artifacts can be handled by providing extra storage slots. This control does not improve rendering quality, and the grid-like artifacts remain visible in the feature maps (Fig. 9a). This suggests that the observed artifacts are not fully explained by the lack of extra storage slots.

Plücker-Only Inference Control. To further localize the source of the grid-like artifacts, we run the decoupled model at inference time with all input RGB values set to zero while keeping the Plücker rays unchanged. As shown in Fig. 8, the intermediate features still exhibit clear network-like grid patterns. Since image appearance has been removed in this control, the remaining artifacts provide evidence that the grid-like patterns are induced by the spatial Plücker-ray representation.

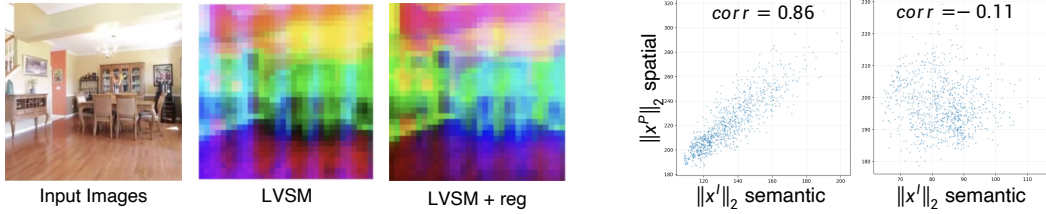
Shared vs. Independent Q/K Projection. We test whether decoupling should also separate query-key (Q/K) routing. In our default block, Q/K are projected from the full token, while values are projected independently from the I -branch and P -branch. The Independent-Q/K variant instead computes Q/K/V separately for the two branches, producing branch-local attention maps, but lowers performance. This suggests that shared Q/K remains useful for spatial coordination, while independent V preserves branch-specific updates (Fig. 7).

Effect of Bidirectional Modulation. We compare modulation in entangled and decoupled representations (Fig. 10). In the entangled model, affine modulation is generated from a mixed feature space, so the scale and shift parameters cannot distinguish whether a response should affect appearance or geometry. In the decoupled model, modulation operates between two specialized branches, allowing spatial tokens to condition appearance tokens and semantic tokens to feed back scene content. The modulation magnitudes in Fig. 11a peak at intermediate layers, where the branches have formed stable representations but still benefit from cross-branch conditioning.

Cross-Branch Modulation Direction. We further ablate the direction of cross-branch conditioning. $P \rightarrow I$ modulation uses spatial tokens to guide appearance rendering, while $I \rightarrow P$ modulation uses updated semantic tokens to refine spatial representations. $P \rightarrow I$ alone is stronger than $I \rightarrow P$ alone, which matches the NVS pipeline where target-view appearance is rendered from viewing geometry. Bidirectional modulation performs best because the second direction provides complementary feedback after the semantic branch has been spatially conditioned. The feature visualizations in Fig. 10 show that this bidirectional design yields more structured representations.

LayerNorm Decoupling. We compare branch-wise LayerNorm with Joint-LN. Joint-LN normalizes the concatenated token using shared statistics, which couples the I -branch and P -branch even after token decoupling. Branch-wise LayerNorm instead normalizes each branch with its own statistics, preserving semantic-spatial separation. As shown in Fig. 9b, Joint-LN produces stronger cross-branch norm correlation, while Separate-LN reduces this coupling and improves reconstruction quality.

Modulation Placement. We study where to insert bidirectional modulation in each block. Applying modulation before attention LayerNorm perturbs the residual stream and leads to unstable training. Applying it after the FFN is stable but weaker, because the nonlinear transformation has already



(a) **Register Tokens Ablation.** Register tokens alone do not remove the grid-like artifacts.

(b) **LayerNorm Ablation.** Entangled representations exhibit strong norm correlation.

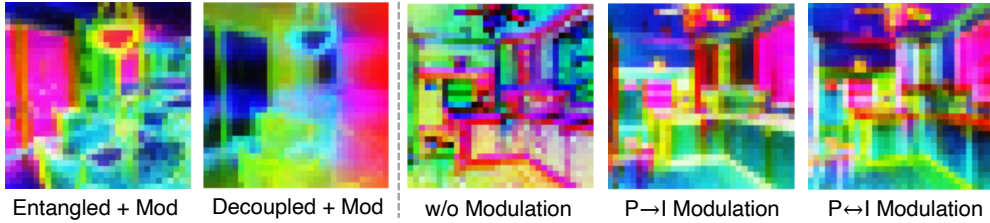
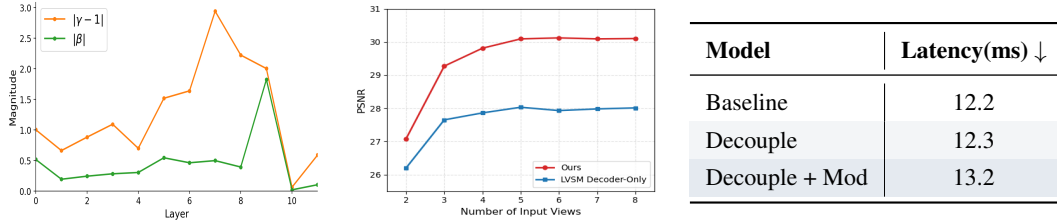


Figure 10: **Entangled vs. Decoupled Modulation and Bidirectional Modulation.** Left: Modulation improves performance in the decoupled structure but degrades performance in the entangled architecture. Right: Bidirectional modulation yields more structured representations.



(a) **Intensity of Modulation.**

(b) **Input-View Generalization.**

(c) **Inference Latency.**

been computed before cross-branch conditioning is introduced. Our final implementation applies modulation after branch-wise LayerNorm and before the branch-specific FFNs, so the generators receive normalized inputs and condition the following nonlinear update.

Generalization to the Number of Input Views. The input-view generalization result in Fig. 11b shows that the design preserves its advantage when the number of test-time input views changes. This suggests that semantic-spatial decoupling improves the underlying representation rather than overfitting to a fixed context size.

4.5 Computational Overhead

We evaluate inference latency under the same setting for all variants, measuring only the model forward pass after warm-up and reporting average per-sample latency. Training-only components, including teacher models, point maps, and auxiliary projection heads, are removed before timing.

As shown in Fig. 11c, base decoupling has nearly the same inference latency as the baseline, because it preserves full-token Q/K attention and does not keep supervision modules at inference. The full model adds only the bidirectional modulation modules, resulting in a modest latency increase. Detailed parameter derivation and timing protocol are provided in Appendix F.

5 Conclusion

We revisited feedforward Transformer-based novel view synthesis and identified that entangling semantic appearance and spatial conditioning within a shared token space induces representational ambiguity and grid-like distortions, which in turn degrade rendering fidelity. To address this, we propose to decouple semantic-spatial features with Independent-V attention that preserves branch purity while retaining controlled cross-stream interaction via shared routing. Extensive experiments and analysis show that the decoupling is effective for feedforward NVS Transformers.

References

- [1] Federico Barbero, Álvaro Arroyo, Xiangming Gu, Christos Perivolaropoulos, Michael Bronstein, Petar Veličković, and Razvan Pascanu. Why do llms attend to the first token? *arXiv preprint arXiv:2504.02732*, 2025.
- [2] Shariq Farooq Bhat, Reiner Birkel, Diana Wofk, Peter Wonka, and Matthias Müller. Zoedepth: Zero-shot transfer by combining relative and metric depth. *arXiv preprint arXiv:2302.12288*, 2023.
- [3] Aleksei Bochkovskii, Amaël Delaunoy, Hugo Germain, Marcel Santos, Yichao Zhou, Stephan R Richter, and Vladlen Koltun. Depth pro: Sharp monocular metric depth in less than a second. *arXiv preprint arXiv:2410.02073*, 2024.
- [4] Mathilde Caron, Hugo Touvron, Ishan Misra, Hervé Jégou, Julien Mairal, Piotr Bojanowski, and Armand Joulin. Emerging properties in self-supervised vision transformers. In *IEEE/CVF International Conference on Computer Vision (ICCV)*, 2021.
- [5] Anpei Chen, Zexiang Xu, Fuqiang Zhao, Xiaoshuai Zhang, Fanbo Xiang, Jingyi Yu, and Hao Su. Mvsnerf: Fast generalizable radiance field reconstruction from multi-view stereo. In *IEEE/CVF International Conference on Computer Vision (ICCV)*, 2021.
- [6] Timothée Darcet, Maxime Oquab, Julien Mairal, and Piotr Bojanowski. Vision transformers need registers. In *International Conference on Learning Representations (ICLR)*, 2024.
- [7] Paul E Debevec, Camillo J Taylor, and Jitendra Malik. Modeling and rendering architecture from photographs: A hybrid geometry- and image-based approach. In *Proceedings of SIGGRAPH*, pages 11–20, 1996.
- [8] Matt Deitke, Dustin Schwenk, Jordi Salvador, Luca Weihs, Oscar Michel, Eli VanderBilt, Ludwig Schmidt, Kiana Ehsani, Aniruddha Kembhavi, and Ali Farhadi. Objaverse: A universe of annotated 3d objects. In *CVPR*, 2023.
- [9] Alexey Dosovitskiy, Lucas Beyer, Alexander Kolesnikov, Dirk Weissenborn, Xiaohua Zhai, Thomas Unterthiner, Mostafa Dehghani, Matthias Minderer, Georg Heigold, Sylvain Gelly, Jakob Uszkoreit, and Neil Houlsby. An image is worth 16x16 words: Transformers for image recognition at scale. In *International Conference on Learning Representations (ICLR)*, 2021.
- [10] Yicong Hong, Kai Zhang, Jiuxiang Gu, Sai Bi, Yang Zhou, Difan Liu, Feng Liu, Kalyan Sunkavalli, Trung Bui, and Hao Tan. Lrm: Large reconstruction model for single image to 3d. In *International Conference on Learning Representations (ICLR)*, 2024.
- [11] Xiaosong Jia, Yihang Sun, Junqi You, Songbur Wong, Zichen Zou, Junchi Yan, Zuxuan Wu, and Yu-Gang Jiang. Efficient-lvsm: Faster, cheaper, and better large view synthesis model via decoupled co-refinement attention. *arXiv preprint arXiv:2602.06478*, 2026.
- [12] Hanwen Jiang, Hao Tan, Peng Wang, Haiyan Jin, Yue Zhao, Sai Bi, Kai Zhang, Fujun Luan, Kalyan Sunkavalli, Qixing Huang, and Georgios Pavlakos. Rayzer: A self-supervised large view synthesis model. *arXiv preprint arXiv:2505.00702*, 2025.
- [13] Haiyan Jin, Hanwen Jiang, Hao Tan, Kai Zhang, Sai Bi, Tianyuan Zhang, Fujun Luan, Noah Snavely, and Zexiang Xu. Lvsm: A large view synthesis model with minimal 3d inductive bias. In *International Conference on Learning Representations (ICLR)*, 2025.
- [14] Justin Johnson, Alexandre Alahi, and Li Fei-Fei. Perceptual losses for real-time style transfer and super-resolution. In *ECCV*, pages 694–711, 2016.
- [15] Gyeongjin Kang, Seungtae Nam, Seungkwon Yang, Xiangyu Sun, Sameh Khamis, Abdelrahman Mohamed, and Eunbyung Park. ilrm: An iterative large 3d reconstruction model, 2025. URL <https://arxiv.org/abs/2507.23277>.
- [16] Bernhard Kerbl, Georgios Kopanas, Thomas Leimkühler, and George Drettakis. 3d gaussian splatting for real-time radiance field rendering. *ACM Transactions on Graphics (TOG)*, 42(4): 1–14, 2023.

- [17] Alexander Lappe and Martin A Giese. Register and [cls] tokens yield a decoupling of local and global features in large vits. *arXiv preprint arXiv:2505.05892*, 2025.
- [18] Xingjian Leng, Jaskirat Singh, Yunzhong Hou, Zhenchang Xing, Saining Xie, and Liang Zheng. Repa-e: Unlocking vae for end-to-end tuning with latent diffusion transformers. *arXiv preprint arXiv:2504.10483*, 2025.
- [19] Haotong Lin, Sili Chen, Junhao Liew, Donny Y Chen, Zhenyu Li, Guang Shi, Jiashi Feng, and Bingyi Kang. Depth anything 3: Recovering the visual space from any views. *arXiv preprint arXiv:2511.10647*, 2025.
- [20] Shikun Liu, Kam Woh Ng, Wonbong Jang, Jiadong Guo, Junlin Han, Haozhe Liu, Yiannis Douratsos, Juan C Pérez, Zijian Zhou, Chi Phung, Tao Xiang, and Juan-Manuel Pérez-Rúa. Scaling sequence-to-sequence generative neural rendering. *arXiv preprint arXiv:2510.04236*, 2025.
- [21] Ilya Loshchilov and Frank Hutter. Decoupled weight decay regularization. In *International Conference on Learning Representations (ICLR)*, 2019.
- [22] Alexis Marouani, Oriane Siméoni, Hervé Jégou, Piotr Bojanowski, and Huy V Vo. Revisiting [cls] and patch token interaction in vision transformers. *arXiv preprint arXiv:2602.08626*, 2026.
- [23] Ben Mildenhall, Pratul P Srinivasan, Matthew Tancik, Jonathan T Barron, Ravi Ramamoorthi, and Ren Ng. Nerf: Representing scenes as neural radiance fields for view synthesis. In *European Conference on Computer Vision (ECCV)*, pages 405–421. Springer, 2020.
- [24] Maxime Oquab, Timothée Darcet, Théo Moutakanni, Huy Vo, Marc Szafraniec, Vasil Khalidov, Pierre Fernandez, Daniel Haziza, Francisco Massa, Alaaeldin El-Nouby, Mahmoud Assran, Nicolas Ballas, Wojciech Galuba, Russell Howes, Po-Yao Huang, Shang-Wen Li, Ishan Misra, Michael Rabbat, Vasu Sharma, Gabriel Synnaeve, Hu Xu, Herve Jegou, Julien Mairal, Patrick Labatut, Armand Joulin, and Piotr Bojanowski. Dinov2: Learning robust visual features without supervision. *arXiv preprint arXiv:2304.07193*, 2023.
- [25] Ethan Perez, Florian Strub, Harm de Vries, Vincent Dumoulin, and Aaron Courville. FiLM: Visual reasoning with a general conditioning layer. In *AAAI Conference on Artificial Intelligence*, pages 3942–3951, 2018.
- [26] Julius Plücker. On a new geometry of space. *Philosophical Transactions of the Royal Society of London*, 155:725–791, 1865.
- [27] Jiawei Shi, Peiyuan Shen, Yinhe Zheng, Lu Hou, Ji Zhang, Yiyang Luo, Xin Xia, Yitong Wang, Chun Yuan, and Hongxia Yang. Denoising vision transformers. In *International Conference on Learning Representations (ICLR)*, 2024.
- [28] Oriane Siméoni, Huy V Vo, Maximilian Seitzer, Federico Baldassarre, Maxime Oquab, Cijo Jose, Vasil Khalidov, Marc Szafraniec, Seungeun Yi, Michaël Ramamonjisoa, Francisco Massa, Daniel Haziza, Luca Wehrstedt, Jianyuan Wang, Timothée Darcet, Théo Moutakanni, Leonel Sentana, Claire Roberts, Andrea Vedaldi, Jamie Tolan, John Brandt, Camille Couprie, Julien Mairal, Hervé Jégou, Patrick Labatut, and Piotr Bojanowski. DINOv3. *arXiv preprint arXiv:2508.10104*, 2025.
- [29] Jaskirat Singh, Xingjian Leng, Zongze Wu, Liang Zheng, Richard Zhang, Eli Shechtman, and Saining Xie. What matters for representation alignment: Global information or spatial structure? *arXiv preprint arXiv:2512.10794*, 2025.
- [30] Yuchuan Tian, Hanting Chen, Mengyu Zheng, Yuchen Liang, Chao Xu, and Yunhe Wang. U-repa: Aligning diffusion u-nets to vits. *arXiv preprint arXiv:2503.18414*, 2025.
- [31] Shinji Umeyama. Least-squares estimation of transformation parameters between two point patterns. *IEEE Transactions on Pattern Analysis and Machine Intelligence*, 13(4):376–380, 1991. doi: 10.1109/34.88573.

- [32] Qianqian Wang, Zhicheng Wang, Kyle Genova, Pratul Srinivasan, Howard Zhou, Jonathan T Barron, Ricardo Martin-Brualla, Noah Snavely, and Thomas Funkhouser. Ibrnet: Learning multi-view image-based rendering. In *IEEE/CVF Conference on Computer Vision and Pattern Recognition (CVPR)*, 2021.
- [33] Ruicheng Wang, Sicheng Xu, Cassie Dai, Jianfeng Xiang, Yu Deng, Xin Tong, and Jiaolong Yang. Moge: Unlocking accurate monocular geometry estimation for open-domain images with optimal training supervision. *arXiv preprint arXiv:2410.19115*, 2024.
- [34] Shuzhe Wang, Vincent Leroy, Yohann Cabon, Boris Chidlovskii, and Jérôme Revaud. Dust3r: Geometric 3d vision made easy. In *IEEE/CVF Conference on Computer Vision and Pattern Recognition (CVPR)*, 2024.
- [35] Zhou Wang, Alan C Bovik, Hamid R Sheikh, and Eero P Simoncelli. Image quality assessment: From error visibility to structural similarity. *IEEE Transactions on Image Processing*, 13(4): 600–612, 2004.
- [36] Zirui Wu, Zeren Jiang, Martin R Oswald, and Jie Song. From rays to projections: Better inputs for feed-forward view synthesis. *arXiv preprint arXiv:2601.05116*, 2026.
- [37] Lihe Yang, Bingyi Kang, Zilong Huang, Xiaogang Xu, Jiashi Feng, and Hengshuang Zhao. Depth anything: Unleashing the power of large-scale unlabeled data. In *IEEE/CVF Conference on Computer Vision and Pattern Recognition (CVPR)*, 2024.
- [38] Lihe Yang, Bingyi Kang, Zilong Huang, Zhen Zhao, Xiaogang Xu, Jiashi Feng, and Hengshuang Zhao. Depth anything v2. *arXiv preprint arXiv:2406.09414*, 2024.
- [39] Alex Yu, Vickie Ye, Matthew Tancik, and Angjoo Kanazawa. pixelnerf: Neural radiance fields from one or few images. In *IEEE/CVF Conference on Computer Vision and Pattern Recognition (CVPR)*, 2021.
- [40] Sihyun Yu, Sangkyung Kwak, Huiwon Jang, Jongheon Jeong, Jonathan Huang, Jinwoo Shin, and Saining Xie. Representation alignment for generation: Training diffusion transformers is easier than you think. *arXiv preprint arXiv:2410.06940*, 2024.
- [41] Kai Zhang, Sai Bi, Hao Tan, Yuanbo Xiangli, Nanxuan Zhao, Kalyan Sunkavalli, and Zexiang Xu. Gs-irm: Large reconstruction model for 3d gaussian splatting. In *European Conference on Computer Vision (ECCV)*, 2024.
- [42] Richard Zhang, Phillip Isola, Alexei A Efros, Eli Shechtman, and Oliver Wang. The unreasonable effectiveness of deep features as a perceptual metric. In *IEEE/CVF Conference on Computer Vision and Pattern Recognition (CVPR)*, pages 586–595, 2018.
- [43] Boyang Zheng, Nanye Ma, Shengbang Tong, and Saining Xie. Diffusion transformers with representation autoencoders. *arXiv preprint arXiv:2510.11690*, 2025.
- [44] Jensen Zhou, Hang Gao, Vikram Voleti, Aaryaman Vasishta, Chun-Han Yao, Mark Boss, Philip Torr, Christian Rupprecht, and Varun Jampani. Stable virtual camera: Generative view synthesis with diffusion models. *arXiv preprint arXiv:2503.14489*, 2025.
- [45] Tinghui Zhou, Richard Tucker, John Flynn, Graham Fyffe, and Noah Snavely. Stereo magnification: Learning view synthesis using multiplane images. In *ACM SIGGRAPH*, 2018.
- [46] Chen Ziwen, Hao Tan, Kai Zhang, Sai Bi, Fujun Luan, Yicong Hong, Fuxin Li, and Zexiang Xu. Long-irm: Long-sequence large reconstruction model for wide-coverage gaussian splats. *arXiv preprint arXiv:2410.12781*, 2024.

A Implementation and Training Details

Controlled Training Budget. The reported baselines are controlled reimplementations rather than numbers copied from the original backbone papers. This setting evaluates the relative effect of semantic-spatial decoupling under a fixed budget; absolute baseline numbers may differ from original reports that use different training scales, model variants, or tuning.

Optimizer and Learning Rate Schedule. All models are trained with AdamW [21] ($\beta_1=0.9$, $\beta_2=0.95$, weight decay 5×10^{-2}). For scene-level training, we use a constant learning rate of 4×10^{-4} with a warm-up of 3 000 iterations. For object-level training, we use the same learning rate with a warm-up of 2 500 iterations. All experiments use mixed precision (BF16).

Dataset-Specific Schedules. For scene-level training on RealEstate10K [45], we use 2 input views and 6 target views, training on 4 A100 80G GPUs with a per-GPU batch size of 4 for 50 K iterations at a resolution of 256×256 . For object-level training on Objaverse [8], we use 4 input views and 8 target views, training on 8 A100 80G GPUs with a per-GPU batch size of 4 for 50 K iterations. All baselines and decoupled variants use the same schedule within each benchmark.

Compute Resources.

Table 3: **Training Compute.** GPU-hours are computed as wall-clock hours multiplied by the number of A100 GPUs.

Experiment	GPUs	Wall-clock time	GPU-hours
RealEstate10K Decoder-Only	4 A100	8 h	32
Objaverse Decoder-Only	8 A100	15 h	120
RealEstate10K Encoder-Decoder	4 A100	12 h	48
RealEstate10K iLRM	4 A100	8 h	32

Loss Weights and Reconstruction Loss. The RGB reconstruction loss \mathcal{L}_{RGB} is a weighted combination of an L2 loss and a VGG perceptual loss [14]:

$$\mathcal{L}_{\text{RGB}} = \mathcal{L}_{\text{L2}} + \lambda_{\text{VGG}} \mathcal{L}_{\text{VGG}}. \quad (13)$$

We set $\lambda_{\text{VGG}}=0.5$ for scene-level training and $\lambda_{\text{VGG}}=1.0$ for object-level training. LPIPS is disabled in the training objective. For supervised variants, the categorized supervision weights are set to $\lambda_I=0.5$ for iREPA supervision and $\lambda_P=0.5$ for geometric consistency.

iREPA Supervision Details. Following iREPA [29], we use DINOv3 ViT-B/16 [28] as the frozen teacher and take its layer-8 output as the alignment target. The student feature is captured from the semantic branch at layer k_I . Before matching, we apply spatial normalization with $\gamma=0.60$ and $\epsilon=10^{-6}$, followed by a lightweight 3×3 convolutional projector that maps the $D/2$ -dimensional semantic feature to the DINOv3 feature dimension. The matching loss is Smooth L1. The projector and DINOv3 teacher are discarded at inference.

Geometric Grounding Details. For each scene or object, training views are processed offline by DA3 [19] to obtain depth maps and camera parameters. We align the DA3 camera coordinates to the training camera coordinates with Umeyama registration [31], back-project the depth maps into 3D point maps, and cache the resulting point maps and validity masks. During training, valid source-view 3D points are projected into target views with the aligned camera parameters, and z-buffering keeps the nearest valid correspondence for each target location. We capture spatial-branch features at layer k_P and apply cosine consistency between corresponding source and target features. View pairs with fewer than 100 valid correspondences are excluded, with the threshold relaxed to 50 for Objaverse. The point maps are used only for training supervision and are not required at inference.

B Supervision Layer Placement

This ablation is performed on the LVSM Decoder-Only model on RealEstate10K. We study the attachment layer of the two optional branch-specific supervision terms introduced in Sec. 3.3. When varying the semantic iREPA layer $k_I \in \{2, 4, 8\}$, we keep the geometric supervision layer fixed at $k_P=10$. When varying the geometric layer $k_P \in \{6, 10, 12\}$, we keep the semantic iREPA layer fixed at $k_I=4$.

Table 4: **Ablation on Supervision Layer Placement.** We vary the layer of semantic iREPA alignment and geometric grounding.

(a) iREPA layer k_I				(b) Geometric layer k_P			
k_I	PSNR \uparrow	SSIM \uparrow	LPIPS \downarrow	k_P	PSNR \uparrow	SSIM \uparrow	LPIPS \downarrow
2	26.51	0.844	0.138	6	26.61	0.843	0.138
4	26.87	0.846	0.136	10	26.87	0.846	0.136
8	26.12	0.840	0.144	12	26.47	0.841	0.140

Geometric supervision fixed at $k_P=10$. iREPA fixed at $k_I=4$.

The best setting is $k_I=4$ and $k_P=10$. Very early supervision can over-constrain low-level features before the two branches have formed stable representations, while very late supervision is closer to the rendering head and provides weaker guidance to intermediate representations.

C Generalization to Encoder-Decoder Architectures

We also evaluate the decoupled design on LVSM Encoder-Decoder. This backbone contains a 12-layer encoder and a 12-layer decoder with hidden dimension $D=768$ and patch size 8. The encoder maps input-view patch tokens and a fixed set of learnable scene tokens into a compact scene representation, and the decoder renders target views from the scene tokens and target-view camera rays.

We keep the same semantic-spatial partition as in the decoder-only model and apply the same decoupled Transformer block described in Sec. 3.2. For input-view tokens, RGB patches initialize the semantic branch (I -branch) and Plücker-ray patches initialize the spatial branch (P -branch). For target tokens, the I -branch is initialized with zeros because no target RGB is observed, while the P -branch is initialized from target-view Plücker rays. The learnable scene tokens use the same D -dimensional interface as the baseline, so the encoder-decoder data flow and rendering head remain unchanged.

The encoder-decoder experiments use the same RealEstate10K training schedule, optimizer, reconstruction objective, and optional branch-specific supervision settings as the decoder-only scene-level experiments in Appendix A. As reported in Table. 1, decoupling improves the LVSM Encoder-Decoder baseline from 24.06 to 25.31 PSNR, showing that the proposed representation is not limited to decoder-only NVS transformers.

D Generalization to the iLRM Architecture

We further apply the decoupled design to iLRM [15], a feed-forward 3D reconstruction model that predicts 3D Gaussian Splatting parameters. Unlike LVSM, iLRM refines image-free Gaussian query tokens through alternating Read blocks and Self-Attention blocks. Read blocks let query tokens attend to context-view support tokens, while Self-Attention blocks propagate interactions among the query tokens.

In our controlled iLRM setting, the processor uses 12 alternating blocks with patch size 8, token dimension 768, and head dimension 64. We decouple both the query stream and the support stream. Query tokens use zero-initialized semantic branches and Plücker-initialized spatial branches; support tokens use RGB patches for the semantic branch and Plücker-ray patches for the spatial branch. The Read and Self-Attention blocks then use the same Independent-V, branch-wise normalization, branch-specific FFN, and bidirectional modulation design described in Sec. 3.2 and Sec. 3.4. The final token is decoded by the original iLRM Gaussian head, leaving the output representation unchanged.

We train the iLRM baseline and decoupled variant on RealEstate10K under the same controlled protocol. We use 2 context views and 4 target views at 256×256 resolution. Both models use AdamW, learning rate 4×10^{-4} , 2 500 warm-up iterations, gradient clipping at 1.0, BF16 mixed precision, 4 A100 80G GPUs, per-GPU batch size 32, and 5 K training iterations. The reconstruction objective follows the iLRM configuration and uses RGB MSE loss. No teacher model, point map, or auxiliary projection head is used at inference.

Under this matched setting, we validate the cross-model effectiveness of the proposed decoupling mechanism on RealEstate10K, with results shown in Table. 5.

Table 5: **Quantitative Comparison on iLRM.** Applying our spatial-semantic decoupled design to iLRM yields improvements.

Model	PSNR \uparrow	SSIM \uparrow	LPIPS \downarrow
iLRM baseline	22.42	0.764	0.276
iLRM-Decoupled (Ours)	23.15	0.789	0.245

E Detailed Visualization

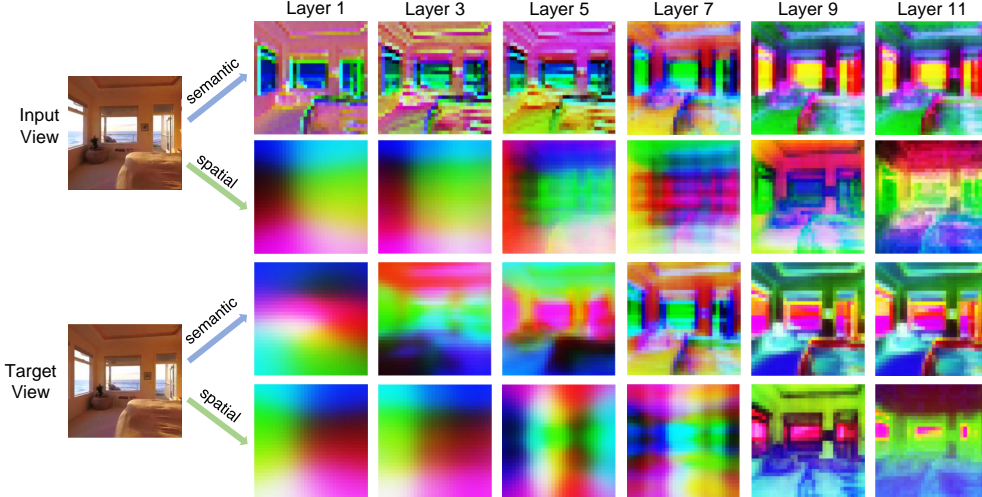


Figure 12: **Layer-wise Feature Visualization of Decouple-Only.** PCA visualizations of intermediate input-view and target-view features from the decouple-only model.

Layer-wise Feature Evolution. Fig. 12 provides PCA visualizations of input-view and target-view features from the decouple-only model across multiple Transformer layers. The visualizations show that the decoupled representation produces organized feature structures throughout the network.

F Inference Complexity Analysis

We provide the parameter derivation for Sec. 4.5. Let D denote the token dimension and r the FFN expansion ratio. Bias terms are omitted because they are lower-order $O(D)$ terms.

Baseline Block. For the entangled baseline, attention uses QKV and output projections, and the FFN uses hidden dimension rD :

$$\mathcal{P}_{\text{attn}}^{\text{base}} = 4D^2, \quad \mathcal{P}_{\text{ffn}}^{\text{base}} = 2rD^2. \quad (14)$$

Thus,

$$\mathcal{P}_{\text{block}}^{\text{base}} = (2r + 4)D^2 + O(D). \quad (15)$$

Base Decoupled Block. In the base decoupled block, Q/K are shared over the full token, while value, output, and FFN transformations are branch-specific:

$$\mathcal{P}_{\text{attn}}^{\text{dec}} = 3D^2, \quad \mathcal{P}_{\text{ffn}}^{\text{dec}} = rD^2. \quad (16)$$

Therefore,

$$\mathcal{P}_{\text{block}}^{\text{dec}} = (r + 3)D^2 + O(D), \quad (17)$$

which is no larger than the baseline block.

LayerNorm and Modulation. Branch-wise LayerNorm preserves parameter count because two full-dimensional LayerNorms are replaced by four half-dimensional LayerNorms:

$$2D = 4 \cdot \frac{D}{2}. \quad (18)$$

Bidirectional modulation adds two FiLM generators:

$$\mathcal{P}_{\text{FiLM}} = 2 \left(\frac{D}{2} \cdot D + D \right) = D^2 + 2D. \quad (19)$$

With $D=768$, this adds about 0.59M parameters per block, or about 7.1M parameters across 12 layers.

Latency Protocol. Latency is measured under the same evaluation setting for all variants. We exclude warm-up batches and report average per-sample forward time. Image saving, metric computation, teacher models, point maps, and auxiliary heads are not included. Categorized supervision therefore does not affect inference latency, while bidirectional modulation adds the only extra inference-time projections.

G Limitations and Future Directions

This work focuses on semantic-spatial representation decoupling under controlled feedforward NVS settings. A natural next step is to study the same representation principle at larger training scales, higher rendering resolutions, and more diverse scene distributions, including longer camera trajectories and more challenging outdoor or dynamic content. Another promising direction is to combine decoupled tokens with alternative camera parameterizations and newer feedforward 3D reconstruction backbones, which may further clarify how semantic appearance and spatial conditioning should interact across model families. Finally, while our branch-specific supervision is removed at inference, future work can explore lighter or fully self-contained training signals that preserve the same semantic-spatial specialization with less offline preprocessing.

H Broader Impacts

Our work improves feedforward novel view synthesis by enhancing the representation of semantic appearance and spatial geometry in Transformer-based models. Potential positive impacts include more efficient 3D content creation, AR/VR applications, robotics simulation, digital twins, and scalable visual scene understanding. By reducing inference overhead, the proposed decoupled design may also make high-quality view synthesis more accessible under limited computational resources.

At the same time, improved view synthesis techniques may be misused to create misleading synthetic visual content, reconstruct private spaces from limited imagery, or generate unauthorized 3D representations of real-world environments. These risks are not unique to our method but are relevant to advances in neural rendering and generative visual modeling. We encourage responsible dataset collection, privacy-preserving deployment, clear disclosure of synthetic content, and appropriate safeguards when applying such systems to real-world or human-centered scenes.

To mitigate these risks, we encourage responsible data collection and deployment practices. Training and evaluation data should be obtained from public, licensed, or consented sources, and applications involving private indoor spaces, identifiable individuals, or sensitive environments should require explicit permission. When view-synthesis outputs are used in downstream applications, synthetic or reconstructed content should be clearly disclosed to users. For code and model release, we plan to provide documentation that describes the intended research use, dataset assumptions, and known limitations, and we discourage applications that enable privacy-invasive reconstruction or misleading visual content generation.

I Existing Assets, Licenses, and Terms

We use existing datasets, model checkpoints, and evaluation assets only for research purposes and cite their original sources. RealEstate10K camera trajectories are released by Google LLC under the Creative Commons Attribution 4.0 International License (CC BY 4.0); the associated video frames are accessed through the standard dataset protocol and remain subject to the original video-source terms. Objaverse is licensed as a dataset under ODC-By v1.0, while individual 3D objects carry per-object Creative Commons licenses recorded in the metadata, including CC BY 4.0, CC BY-NC 4.0, CC BY-NC-SA 4.0, CC BY-SA 4.0, and CC0 1.0. We use Objaverse assets and derived renderings according to their metadata licenses and do not redistribute the original assets.

For auxiliary supervision, we use DINOv3 ViT-B/16 under the DINOv3 License and the DA3NESTED-GIANT-LARGE checkpoint under the Creative Commons Attribution-NonCommercial 4.0 International License (CC BY-NC 4.0). The DA3 code repository is released

under Apache-2.0. These external models are used only to generate training-time supervision; their checkpoints, intermediate caches, and teacher outputs are not redistributed with this submission. Baseline methods and evaluation protocols are credited through citations to the corresponding papers.

NeurIPS Paper Checklist

1. Claims

Question: Do the main claims made in the abstract and introduction accurately reflect the paper’s contributions and scope?

Answer: [Yes]

Justification: The abstract and introduction state the semantic–spatial decoupling contribution, the optional supervision and modulation components, and the controlled experimental scope. The claims are supported by the method description and experiments in Sections 3 and 4.

Guidelines:

- The answer [N/A] means that the abstract and introduction do not include the claims made in the paper.
- The abstract and/or introduction should clearly state the claims made, including the contributions made in the paper and important assumptions and limitations. A [No] or [N/A] answer to this question will not be perceived well by the reviewers.
- The claims made should match theoretical and experimental results, and reflect how much the results can be expected to generalize to other settings.
- It is fine to include aspirational goals as motivation as long as it is clear that these goals are not attained by the paper.

2. Limitations

Question: Does the paper discuss the limitations of the work performed by the authors?

Answer: [Yes]

Justification: The appendix includes a Limitations and Future Directions section discussing scale, resolution, dataset diversity, camera parameterizations, and lighter training supervision as future directions.

Guidelines:

- The answer [N/A] means that the paper has no limitation while the answer [No] means that the paper has limitations, but those are not discussed in the paper.
- The authors are encouraged to create a separate “Limitations” section in their paper.
- The paper should point out any strong assumptions and how robust the results are to violations of these assumptions (e.g., independence assumptions, noiseless settings, model well-specification, asymptotic approximations only holding locally). The authors should reflect on how these assumptions might be violated in practice and what the implications would be.
- The authors should reflect on the scope of the claims made, e.g., if the approach was only tested on a few datasets or with a few runs. In general, empirical results often depend on implicit assumptions, which should be articulated.
- The authors should reflect on the factors that influence the performance of the approach. For example, a facial recognition algorithm may perform poorly when image resolution is low or images are taken in low lighting. Or a speech-to-text system might not be used reliably to provide closed captions for online lectures because it fails to handle technical jargon.
- The authors should discuss the computational efficiency of the proposed algorithms and how they scale with dataset size.
- If applicable, the authors should discuss possible limitations of their approach to address problems of privacy and fairness.
- While the authors might fear that complete honesty about limitations might be used by reviewers as grounds for rejection, a worse outcome might be that reviewers discover limitations that aren’t acknowledged in the paper. The authors should use their best judgment and recognize that individual actions in favor of transparency play an important role in developing norms that preserve the integrity of the community. Reviewers will be specifically instructed to not penalize honesty concerning limitations.

3. Theory assumptions and proofs

Question: For each theoretical result, does the paper provide the full set of assumptions and a complete (and correct) proof?

Answer: [N/A]

Justification: The paper does not present theoretical results, theorems, or formal proofs; its contribution is architectural and empirical.

Guidelines:

- The answer [N/A] means that the paper does not include theoretical results.
- All the theorems, formulas, and proofs in the paper should be numbered and cross-referenced.
- All assumptions should be clearly stated or referenced in the statement of any theorems.
- The proofs can either appear in the main paper or the supplemental material, but if they appear in the supplemental material, the authors are encouraged to provide a short proof sketch to provide intuition.
- Inversely, any informal proof provided in the core of the paper should be complemented by formal proofs provided in appendix or supplemental material.
- Theorems and Lemmas that the proof relies upon should be properly referenced.

4. Experimental result reproducibility

Question: Does the paper fully disclose all the information needed to reproduce the main experimental results of the paper to the extent that it affects the main claims and/or conclusions of the paper (regardless of whether the code and data are provided or not)?

Answer: [Yes]

Justification: The method and appendix specify the architecture, losses, supervision construction, datasets, metrics, training schedules, and compute needed to reproduce the main experimental setting.

Guidelines:

- The answer [N/A] means that the paper does not include experiments.
- If the paper includes experiments, a [No] answer to this question will not be perceived well by the reviewers: Making the paper reproducible is important, regardless of whether the code and data are provided or not.
- If the contribution is a dataset and/or model, the authors should describe the steps taken to make their results reproducible or verifiable.
- Depending on the contribution, reproducibility can be accomplished in various ways. For example, if the contribution is a novel architecture, describing the architecture fully might suffice, or if the contribution is a specific model and empirical evaluation, it may be necessary to either make it possible for others to replicate the model with the same dataset, or provide access to the model. In general, releasing code and data is often one good way to accomplish this, but reproducibility can also be provided via detailed instructions for how to replicate the results, access to a hosted model (e.g., in the case of a large language model), releasing of a model checkpoint, or other means that are appropriate to the research performed.
- While NeurIPS does not require releasing code, the conference does require all submissions to provide some reasonable avenue for reproducibility, which may depend on the nature of the contribution. For example
 - (a) If the contribution is primarily a new algorithm, the paper should make it clear how to reproduce that algorithm.
 - (b) If the contribution is primarily a new model architecture, the paper should describe the architecture clearly and fully.
 - (c) If the contribution is a new model (e.g., a large language model), then there should either be a way to access this model for reproducing the results or a way to reproduce the model (e.g., with an open-source dataset or instructions for how to construct the dataset).
 - (d) We recognize that reproducibility may be tricky in some cases, in which case authors are welcome to describe the particular way they provide for reproducibility. In the case of closed-source models, it may be that access to the model is limited in

some way (e.g., to registered users), but it should be possible for other researchers to have some path to reproducing or verifying the results.

5. Open access to data and code

Question: Does the paper provide open access to the data and code, with sufficient instructions to faithfully reproduce the main experimental results, as described in supplemental material?

Answer: [Yes]

Justification: We use public datasets, and all baseline methods are open-source. We plan to release our code upon paper acceptance.

Guidelines:

- The answer [N/A] means that paper does not include experiments requiring code.
- Please see the NeurIPS code and data submission guidelines (<https://neurips.cc/public/guides/CodeSubmissionPolicy>) for more details.
- While we encourage the release of code and data, we understand that this might not be possible, so [No] is an acceptable answer. Papers cannot be rejected simply for not including code, unless this is central to the contribution (e.g., for a new open-source benchmark).
- The instructions should contain the exact command and environment needed to run to reproduce the results. See the NeurIPS code and data submission guidelines (<https://neurips.cc/public/guides/CodeSubmissionPolicy>) for more details.
- The authors should provide instructions on data access and preparation, including how to access the raw data, preprocessed data, intermediate data, and generated data, etc.
- The authors should provide scripts to reproduce all experimental results for the new proposed method and baselines. If only a subset of experiments are reproducible, they should state which ones are omitted from the script and why.
- At submission time, to preserve anonymity, the authors should release anonymized versions (if applicable).
- Providing as much information as possible in supplemental material (appended to the paper) is recommended, but including URLs to data and code is permitted.

6. Experimental setting/details

Question: Does the paper specify all the training and test details (e.g., data splits, hyperparameters, how they were chosen, type of optimizer) necessary to understand the results?

Answer: [Yes]

Justification: Sections 4 and A specify datasets, splits/protocols, view counts, resolution, optimizer, loss weights, batch sizes, training iterations, and evaluation metrics.

Guidelines:

- The answer [N/A] means that the paper does not include experiments.
- The experimental setting should be presented in the core of the paper to a level of detail that is necessary to appreciate the results and make sense of them.
- The full details can be provided either with the code, in appendix, or as supplemental material.

7. Experiment statistical significance

Question: Does the paper report error bars suitably and correctly defined or other appropriate information about the statistical significance of the experiments?

Answer: [No]

Justification: Due to computational cost, each configuration is trained once under the same controlled setting. We therefore interpret the ablations by consistent trends across metrics, architectures, and datasets rather than statistical significance.

Guidelines:

- The answer [N/A] means that the paper does not include experiments.

- The authors should answer [Yes] if the results are accompanied by error bars, confidence intervals, or statistical significance tests, at least for the experiments that support the main claims of the paper.
- The factors of variability that the error bars are capturing should be clearly stated (for example, train/test split, initialization, random drawing of some parameter, or overall run with given experimental conditions).
- The method for calculating the error bars should be explained (closed form formula, call to a library function, bootstrap, etc.)
- The assumptions made should be given (e.g., Normally distributed errors).
- It should be clear whether the error bar is the standard deviation or the standard error of the mean.
- It is OK to report 1-sigma error bars, but one should state it. The authors should preferably report a 2-sigma error bar than state that they have a 96% CI, if the hypothesis of Normality of errors is not verified.
- For asymmetric distributions, the authors should be careful not to show in tables or figures symmetric error bars that would yield results that are out of range (e.g., negative error rates).
- If error bars are reported in tables or plots, the authors should explain in the text how they were calculated and reference the corresponding figures or tables in the text.

8. Experiments compute resources

Question: For each experiment, does the paper provide sufficient information on the computer resources (type of compute workers, memory, time of execution) needed to reproduce the experiments?

Answer: [Yes]

Justification: Appendix A and Table 3 report GPU type, GPU count, wall-clock training time, and GPU-hours for the reported training settings.

Guidelines:

- The answer [N/A] means that the paper does not include experiments.
- The paper should indicate the type of compute workers CPU or GPU, internal cluster, or cloud provider, including relevant memory and storage.
- The paper should provide the amount of compute required for each of the individual experimental runs as well as estimate the total compute.
- The paper should disclose whether the full research project required more compute than the experiments reported in the paper (e.g., preliminary or failed experiments that didn't make it into the paper).

9. Code of ethics

Question: Does the research conducted in the paper conform, in every respect, with the NeurIPS Code of Ethics <https://neurips.cc/public/EthicsGuidelines>?

Answer: [Yes]

Justification: The work uses existing research datasets and model checkpoints with citations and license/terms disclosure, and does not involve human subjects, crowdsourcing, or a deployment that raises special ethics concerns.

Guidelines:

- The answer [N/A] means that the authors have not reviewed the NeurIPS Code of Ethics.
- If the authors answer [No], they should explain the special circumstances that require a deviation from the Code of Ethics.
- The authors should make sure to preserve anonymity (e.g., if there is a special consideration due to laws or regulations in their jurisdiction).

10. Broader impacts

Question: Does the paper discuss both potential positive societal impacts and negative societal impacts of the work performed?

Answer: [Yes]

Justification: See Appendix H.

Guidelines:

- The answer [N/A] means that there is no societal impact of the work performed.
- If the authors answer [N/A] or [No], they should explain why their work has no societal impact or why the paper does not address societal impact.
- Examples of negative societal impacts include potential malicious or unintended uses (e.g., disinformation, generating fake profiles, surveillance), fairness considerations (e.g., deployment of technologies that could make decisions that unfairly impact specific groups), privacy considerations, and security considerations.
- The conference expects that many papers will be foundational research and not tied to particular applications, let alone deployments. However, if there is a direct path to any negative applications, the authors should point it out. For example, it is legitimate to point out that an improvement in the quality of generative models could be used to generate Deepfakes for disinformation. On the other hand, it is not needed to point out that a generic algorithm for optimizing neural networks could enable people to train models that generate Deepfakes faster.
- The authors should consider possible harms that could arise when the technology is being used as intended and functioning correctly, harms that could arise when the technology is being used as intended but gives incorrect results, and harms following from (intentional or unintentional) misuse of the technology.
- If there are negative societal impacts, the authors could also discuss possible mitigation strategies (e.g., gated release of models, providing defenses in addition to attacks, mechanisms for monitoring misuse, mechanisms to monitor how a system learns from feedback over time, improving the efficiency and accessibility of ML).

11. Safeguards

Question: Does the paper describe safeguards that have been put in place for responsible release of data or models that have a high risk for misuse (e.g., pre-trained language models, image generators, or scraped datasets)?

Answer: [Yes]

Justification: See Appendix H.

Guidelines:

- The answer [N/A] means that the paper poses no such risks.
- Released models that have a high risk for misuse or dual-use should be released with necessary safeguards to allow for controlled use of the model, for example by requiring that users adhere to usage guidelines or restrictions to access the model or implementing safety filters.
- Datasets that have been scraped from the Internet could pose safety risks. The authors should describe how they avoided releasing unsafe images.
- We recognize that providing effective safeguards is challenging, and many papers do not require this, but we encourage authors to take this into account and make a best faith effort.

12. Licenses for existing assets

Question: Are the creators or original owners of assets (e.g., code, data, models), used in the paper, properly credited and are the license and terms of use explicitly mentioned and properly respected?

Answer: [Yes]

Justification: The appendix includes an Existing Assets, Licenses, and Terms section covering RealEstate10K, Objaverse, DINOv3, DA3, and credited baseline/evaluation assets.

Guidelines:

- The answer [N/A] means that the paper does not use existing assets.
- The authors should cite the original paper that produced the code package or dataset.

- The authors should state which version of the asset is used and, if possible, include a URL.
- The name of the license (e.g., CC-BY 4.0) should be included for each asset.
- For scraped data from a particular source (e.g., website), the copyright and terms of service of that source should be provided.
- If assets are released, the license, copyright information, and terms of use in the package should be provided. For popular datasets, paperswithcode.com/datasets has curated licenses for some datasets. Their licensing guide can help determine the license of a dataset.
- For existing datasets that are re-packaged, both the original license and the license of the derived asset (if it has changed) should be provided.
- If this information is not available online, the authors are encouraged to reach out to the asset’s creators.

13. New assets

Question: Are new assets introduced in the paper well documented and is the documentation provided alongside the assets?

Answer: [N/A]

Justification: The paper does not introduce or release a new dataset, code package, or model asset; it uses existing assets and reports experimental results.

Guidelines:

- The answer [N/A] means that the paper does not release new assets.
- Researchers should communicate the details of the dataset/code/model as part of their submissions via structured templates. This includes details about training, license, limitations, etc.
- The paper should discuss whether and how consent was obtained from people whose asset is used.
- At submission time, remember to anonymize your assets (if applicable). You can either create an anonymized URL or include an anonymized zip file.

14. Crowdsourcing and research with human subjects

Question: For crowdsourcing experiments and research with human subjects, does the paper include the full text of instructions given to participants and screenshots, if applicable, as well as details about compensation (if any)?

Answer: [N/A]

Justification: The work does not involve crowdsourcing experiments or research with human subjects.

Guidelines:

- The answer [N/A] means that the paper does not involve crowdsourcing nor research with human subjects.
- Including this information in the supplemental material is fine, but if the main contribution of the paper involves human subjects, then as much detail as possible should be included in the main paper.
- According to the NeurIPS Code of Ethics, workers involved in data collection, curation, or other labor should be paid at least the minimum wage in the country of the data collector.

15. Institutional review board (IRB) approvals or equivalent for research with human subjects

Question: Does the paper describe potential risks incurred by study participants, whether such risks were disclosed to the subjects, and whether Institutional Review Board (IRB) approvals (or an equivalent approval/review based on the requirements of your country or institution) were obtained?

Answer: [N/A]

Justification: The work does not involve crowdsourcing or human-subject research, so IRB approval or equivalent review is not applicable.

Guidelines:

- The answer [N/A] means that the paper does not involve crowdsourcing nor research with human subjects.
- Depending on the country in which research is conducted, IRB approval (or equivalent) may be required for any human subjects research. If you obtained IRB approval, you should clearly state this in the paper.
- We recognize that the procedures for this may vary significantly between institutions and locations, and we expect authors to adhere to the NeurIPS Code of Ethics and the guidelines for their institution.
- For initial submissions, do not include any information that would break anonymity (if applicable), such as the institution conducting the review.

16. **Declaration of LLM usage**

Question: Does the paper describe the usage of LLMs if it is an important, original, or non-standard component of the core methods in this research? Note that if the LLM is used only for writing, editing, or formatting purposes and does *not* impact the core methodology, scientific rigor, or originality of the research, declaration is not required.

Answer: [N/A]

Justification: We use LLM for writing and formatting. The core method does not use LLMs as an important, original, or non-standard research component.

Guidelines:

- The answer [N/A] means that the core method development in this research does not involve LLMs as any important, original, or non-standard components.
- Please refer to our LLM policy in the NeurIPS handbook for what should or should not be described.